

Award Number: W81XWH-04-1-0461

TITLE: Time-Resolved and Spectroscopic Three-Dimensional Optical Breast Tomography

PRINCIPAL INVESTIGATOR: Robert R. Alfano, Ph.D.
S. K. Gayen, Ph.D.

CONTRACTING ORGANIZATION: City College of New York
New York, NY 10031

REPORT DATE: April 2008

TYPE OF REPORT: Annual

PREPARED FOR: U.S. Army Medical Research and Materiel Command
Fort Detrick, Maryland 21702-5012

DISTRIBUTION STATEMENT: Approved for Public Release;
Distribution Unlimited

The views, opinions and/or findings contained in this report are those of the author(s) and should not be construed as an official Department of the Army position, policy or decision unless so designated by other documentation.

REPORT DOCUMENTATION PAGE

Form Approved
OMB No. 0704-0188

Public reporting burden for this collection of information is estimated to average 1 hour per response, including the time for reviewing instructions, searching existing data sources, gathering and maintaining the data needed, and completing and reviewing this collection of information. Send comments regarding this burden estimate or any other aspect of this collection of information, including suggestions for reducing this burden to Department of Defense, Washington Headquarters Services, Directorate for Information Operations and Reports (0704-0188), 1215 Jefferson Davis Highway, Suite 1204, Arlington, VA 22202-4302. Respondents should be aware that notwithstanding any other provision of law, no person shall be subject to any penalty for failing to comply with a collection of information if it does not display a currently valid OMB control number. **PLEASE DO NOT RETURN YOUR FORM TO THE ABOVE ADDRESS.**

1. REPORT DATE (DD-MM-YYYY) 01-04-2008			2. REPORT TYPE Annual			3. DATES COVERED (From - To) 1 APR 2007 - 31 MAR 2008			
4. TITLE AND SUBTITLE Time-Resolved and Spectroscopic Three-Dimensional Optical Breast Tomography						5a. CONTRACT NUMBER			
						5b. GRANT NUMBER W81XWH-04-1-0461			
						5c. PROGRAM ELEMENT NUMBER			
6. AUTHOR(S) Robert R. Alfano, Ph.D.; S. K. Gayen, Ph.D. E-Mail: alfano@sci.cuny.cuny.edu						5d. PROJECT NUMBER			
						5e. TASK NUMBER			
						5f. WORK UNIT NUMBER			
7. PERFORMING ORGANIZATION NAME(S) AND ADDRESS(ES) City College of New York New York, NY 10031						8. PERFORMING ORGANIZATION REPORT NUMBER			
9. SPONSORING / MONITORING AGENCY NAME(S) AND ADDRESS(ES) U.S. Army Medical Research and Materiel Command Fort Detrick, Maryland 21702-5012						10. SPONSOR/MONITOR'S ACRONYM(S)			
						11. SPONSOR/MONITOR'S REPORT NUMBER(S)			
12. DISTRIBUTION / AVAILABILITY STATEMENT Approved for Public Release; Distribution Unlimited									
13. SUPPLEMENTARY NOTES									
14. ABSTRACT The research carried out during the current reporting period included: (a) application and further refinement of optical tomographic imaging using independent component analysis (OPTICA) developed during the earlier reporting periods for locating and cross-section imaging of a tumor in a model cancerous breast assembled using ex vivo breast tissue specimens; and (b) development of a new approach for detection of a target in a highly scattering turbid medium using near-infrared center of intensity time gated imaging. The OPTICA approach was able to detect, provide the location with an accuracy of ~ 1 mm and cross section of the tumor in the model cancerous breast. It also identified two streaks of fibro-glandular tissues in the breast. The near-infrared center of intensity time gated imaging approach provided two-dimensional image of a piece of porcine liver within a slab of porcine tissue, and shows promise to evolve as a simple optical biomedical imaging approach.									
15. SUBJECT TERMS Breast cancer, near-infrared imaging, fluorescence imaging, tomography, target localization, optical tomography using independent component analysis (OPTICA)									
16. SECURITY CLASSIFICATION OF:						17. LIMITATION OF ABSTRACT	18. NUMBER OF PAGES	19a. NAME OF RESPONSIBLE PERSON USAMRMC	
a. REPORT U	b. ABSTRACT U	c. THIS PAGE U	19b. TELEPHONE NUMBER (include area code)						
						UU	29		

Table of Contents

	Page
Introduction.....	4
Body.....	4
Key Research Accomplishments.....	6
Reportable Outcomes.....	7
Conclusions.....	7
References.....	8
Appendices.....	9

4. INTRODUCTION

The research project, “Time-Resolved and Spectroscopic Three-Dimensional Optical Breast Tomography,” is devoted to developing a safe and affordable breast cancer detection modality that makes use of noninvasive near-infrared (NIR) light for imaging, locating and diagnosing tumors in human breast with high resolution and specificity. The research focuses on the development and application of: (a) experimental approaches for probing the target using NIR light, and (b) image reconstruction and target localization algorithms for obtaining target location and generating three-dimensional (3-D) tomographic images.

Significant progress has been made in both the areas during the reporting period (May 1, 2007 – April 30, 2008) covered by this report.

5. BODY

The tasks performed and the progresses made during the current reporting period are as follows:

- Application and further refinement of optical tomographic imaging using independent component analysis (OPTICA) developed during the earlier reporting periods for locating and cross-section imaging of a tumor in a model breast constructed using *ex vivo* breast tissue specimens;
- Development of a new approach for detection of a target in a highly scattering turbid medium using near-infrared center of intensity time gated imaging.

We provide a brief outline of our accomplishments in these areas, and refer to appended publications for detailed description where applicable.

5.1. Detection, localization, and cross section imaging of model cancerous breast using OPTICA

We have pursued further improvement and testing of OPTICA (optical tomographic imaging using independent component analysis) that was developed^{1,2} and reported during the earlier reporting periods.^{3,4} Particular emphasis was placed on testing the efficacy of the experimental arrangement, theoretical model, and numerical algorithm to detect, locate, and image a tumor inside a cancerous breast (*TO 1, Task 2; TO 2, Task 4; and TO 4, Task 9*). These are detailed in *Appendix 1: “Optical diffuse imaging of an *ex vivo* model cancerous human breast using independent component analysis,” IEEE J. Select. Topics Quantum Electron. 14, 43 (2008).*

At our present state of development OPTICA can detect an optical inhomogeneity (such as, a tumor) inside a highly scattering turbid medium (such as, a human breast) based on a difference in optical absorption, fluorescence, or scattering characteristics.^{1,2,5} The multi-source probing and multi-detector monitoring scheme used in OPTICA provides multiple angular views of the target and enable determination of the position of the target with high accuracy (typically within 1 mm). The formalism has been further extended to provide cross sectional image of a target within a turbid medium.^{5,6}

We will provide a brief overview of a measurement on a realistic cancerous breast model and leave the details to a recent appended reprint (*Appendix 1*). The model breast was a 70 mm X 55 mm X 33 mm slab composed of two pieces of *ex vivo* human breast tissues provided to us by National Disease Research Interchange under an Internal Review Board approval at the City

College of New York. The larger piece was normal tissue that included mainly adipose tissue and streaks of fibro-glandular tissues. The existence of the fibro-glandular tissues was not known prior to making the measurements. The second piece was mainly a tumor (infiltrating ductal carcinoma) with a small amount of normal tissues in the margins with an overall approximate dimension of 8 mm X 5 mm X 3 mm. An incision was made in the mid-plane (along the z -axis, which was the shorter dimension of the tissue) of the normal piece and some amount of normal tissue was removed from the central region making a small pouch. The tumor piece was then inserted into the pouch and the incision was closed by moderate compression of the composite consisting of the normal tissue and the tumor along x - y - z directions. The breast tissue slab was contained inside a transparent plastic box. One of the sides of the box could be moved to uniformly compress the tissue along the z -axis and hold it in position. The resulting specimen, a 70 mm X 55 mm X 33 mm slab, was treated as one entity in the subsequent imaging experiment. The position of the tumor within the slab was known since it was placed in position as discussed above. One of the tests of the efficacy of this imaging approach was to see how well the known position is assessed.

The experimental arrangement (shown schematically in Fig. 1(a) of *Appendix 1*) used a 200- μm optical fiber to deliver a 784-nm, 300 mW continuous-wave beam from a diode laser for sample illumination. The beam was collimated to a 1-mm spot onto the entrance face (the ‘source plane’) of the slab sample. Multiple source illumination was realized in practice by step scanning the slab sample across the laser beam in a 22X 16 x - y array of grid points with a step size of 2.0 mm using a computer controlled translation stage. The signal from the opposite face of the sample (the ‘detection plane’) was collected by a camera lens and projected onto the sensing element of a cooled 16-bit, 1024 X 1024-pixel charged couple device (CCD) camera. Although the scanned area is 42 mm X 30 mm on the source plane, the imaged area of the detection plane was much larger, covering the entire 70 mm X 55 mm area of the model breast. Each illuminated pixel of the CCD camera could be regarded as a detector.

For illumination of each scanned point, the CCD camera recorded an image. A typical raw image is shown in Fig. 1(c) of *Appendix 1*. Each raw image was then cropped to select out the information-rich region, and binned to enhance the signal-to-noise ratio. All the binned images corresponding to illumination of the grid points in sequence were then stacked, and used as input for independent component analysis. The details of the analysis method, theoretical formalism, target localization algorithm, and experimental arrangement have been published,⁶ and are presented in *Appendix 1*. After optical measurements, the sample was transferred to our collaborators at the New York Eye and Ear Infirmary for pathological study and correlation (*TO2, Task 5*).

The key results of the experiment are as follows.

(a) OPTICA identified three different structures (Fig. 2, *Appendix 1*) as three independent components based on the differences in optical properties. These include the tumor whose presence and position was known from the sample preparation process. We ascribed the other two structures to fibro-glandular tissues, as the normal component of the breast tissue specimen was mainly adipose tissue. Comparison with the pathology results further confirmed the identity of the tumor and the fibro-glandular tissues.

(b) The location of the tumor was determined to within ~ 1 mm in all three dimensions. The locations of the fibro-glandular tissues were also estimated. The locations of the components are given in Table I of *Appendix 1*.

(c) The FWHM of the tumor is estimated to be ~ 10.3 mm and 7.4 mm along the x and y directions, respectively (details in Fig. 3, *Appendix 1*).

5.2 Development of near-infrared center of intensity time gated imaging approach

A major thrust of the project is to develop optical imaging approaches that are simple and easy to implement. During the present reporting period we have explored the development of a new near-infrared optical imaging approach for locating a target embedded in a turbid medium. The approach is based on the premise that a target (that is, an optical inhomogeneity) within the turbid medium alters the propagation of light through the medium. Consequently, the spatial distribution of the output light intensity (SDOLI) is different with an embedded target than that without it. The target localization is based on an analysis of the spatial variation of the transmitted light intensity distribution for illumination at different positions on the sample boundary. The basic principle, experimental arrangement, and preliminary results are presented in *Appendix 2* (“*Detection of a target in a highly scattering turbid medium using near-infrared center of intensity time gated imaging*”), in the form of a manuscript to be submitted for publication.

The experimental arrangement for realizing the approach in practice is shown in Fig. 2 of *Appendix 2*. The scattering medium was a suspension of Intralipid-10% in water, with an estimated reduced scattering coefficient, $\mu_s \sim 1.168 \text{ mm}^{-1}$ (transport length 0.86 mm) and an absorption coefficient of 0.0021 mm^{-1} at 800 nm. The Intralipid-10% suspension was held in a 240 mm x 160 mm x 65 mm rectangular glass container. The target was a 10 mm x 10 mm x 3 mm neutral density filter (absorption coefficient 0.23 mm^{-1} at 800 nm). Another sample was a 5 mm x 5 mm x 5 mm piece of porcine liver (target) placed inside a 150 mm x 90 mm x 50 mm slab of porcine tissue held in a rectangular plastic cell.

The samples were illuminated by 800 nm, 200 ps, 1 kHz repetition rate pulses from a Ti:sapphire laser and regenerative amplifier system. The average beam power was 150 mW and the beam spot size was approximately 2 mm. The laser beam was incident along the z -axis into one of the 240 mm x 160 mm flat faces of the container. The 2- D intensity distribution of light emergent from the opposite end face of the cell was recorded by an ultrafast gated intensified camera system (UGICS). The UGICS provides an electronic time gate whose full width at half maximum (FWHM) duration can be set as short as 80 ps. The gate position could be varied over a 20 ns range with a minimum step size of 25 ps. The sample cell was mounted on a translation stage for lateral scanning. The input beam and the UGICS were not scanned.

The approach was able to detect the target in both the cases. As shown in Fig. 5 of *Appendix 2*, the approach provided a two-dimensional image of the porcine liver embedded within the porcine tissue.

6. KEY RESEARCH ACCOMPLISHMENTS

- Demonstrated the efficacy of Optical Tomography using Independent Component Analysis (OPTICA) approach for detection, 3-D localization, and cross section imaging of a tumor inside a realistic breast model composed of excised breast tissues was determined with millimeter accuracy (*Appendix 1*).

- Developed a new approach for obtaining two-dimensional image of a target embedded inside a turbid medium (*Appendix 2*).

7. REPORTABLE OUTCOMES

Journal Articles

1. M. Xu, M. Alrubaiee, S. K. Gayen and R. R. Alfano, “Optical diffuse imaging of an *ex vivo* model cancerous human breast using independent component analysis,” *IEEE J. Select. Topics Quantum Electron.* **14**, 43 (2008).

Presentations

2. M. Alrubaiee, S. K. Gayen, and R. R. Alfano, “Near-infrared time-resolved and spectroscopic imaging for breast cancer detection.” Poster P42-17 presented at the *Era of Hope*, Department of Defense Breast Cancer Research Program Meeting, June 25-28, 2008, Baltimore, Maryland. Abstract appears in p. 293 of Meeting Proceedings.
3. M. Xu, M. Alrubaiee, S. K. Gayen, and R. R. Alfano, “Optical tomography using independent component analysis.” Poster P42-17 presented at the *Era of Hope*, Department of Defense Breast Cancer Research Program Meeting, June 25-28, 2008, Baltimore, Maryland. Abstract appears in p. 292 of Meeting Proceedings.

8. CONCLUSION

The work carried out during this reporting period shows the potential for detection and three-dimensional localization of a tumor within a breast with significant accuracy based on the differences in the scattering and absorption characteristics of the tumor and normal breast tissue.

“So What Section”

- A recent study involving 35,319 patients underscores the influence of primary tumor location on breast cancer prognosis, and makes it imperative that breast cancer detection modalities obtain three dimensional (3-D) location of the tumor relative to the axilla.⁷ The current work is an important development in obtaining noninvasive 3-D location of a tumor within the breast.
- Three-dimensional target localization will enable closer probing of a smaller volume around of the target providing more details since smaller pixel size could be used without increasing the computation time (as a smaller volume will be probed).
- What is more important, the work accomplished so far prepares us for the next step, *in vivo* optical breast imaging involving volunteers.

9. REFERENCES

1. M. Xu, M. Alrubaiee, S. K. Gayen and R. R. Alfano, "Three-dimensional optical imaging of objects in a turbid medium using independent component analysis: theory and simulation," *J. Biomed. Opt.* **10**, 051705 (2005).
2. M. Alrubaiee, M. Xu, S. K. Gayen, M. Brito, and R. R. Alfano, "Three-dimensional optical tomographic imaging of objects in tissue-simulating turbid medium using independent component analysis," *Appl. Phys. Lett.* **87**, 191112 (2005).
3. First technical report of this project covering the period 5/1/2004 – 4/30/2006.
4. Second technical report of this project covering the period 5/1/2006 – 4/30/2007.
5. M. Alrubaiee, M. Xu, S. K. Gayen, and R. R. Alfano, "Three-dimensional localization and cross section reconstruction of fluorescent targets in *ex vivo* breast tissue using independent component analysis," *Appl. Phys. Lett.* **89**, 133902 (2006).
6. M. Xu, M. Alrubaiee, S. K. Gayen and R. R. Alfano, "Optical diffuse imaging of an *ex vivo* model cancerous human breast using independent component analysis," *IEEE J. Select. Topics Quantum Electron.* **14**, 43 (2008).
7. N. Kroman, J. Wohlfahrt, H. T. Mouridsen, and M. Melbye, "Influence of tumor location on breast cancer prognosis," *Int. J. Cancer* **105**, 542 -545 (2003).

10. APPENDICES

- Appendix 1.* M. Xu, M. Alrubaiee, S. K. Gayen and R. R. Alfano, “Optical diffuse imaging of an *ex vivo* model cancerous human breast using independent component analysis,” *IEEE J. Select. Topics Quantum Electron.* **14**, 43 (2008).
- Appendix 2.* Yimin Wang, M. Alrubaiee, S. K. Gayen, and R. R. Alfano, “Detection of a target in a highly scattering turbid medium using near-infrared center of intensity time gated imaging,” *Optics Communications* (to be submitted).

Optical Diffuse Imaging of an *Ex Vivo* Model Cancerous Human Breast Using Independent Component Analysis

Min Xu, Mohammad Alrubaiee, S. K. Gayen, and R. R. Alfano, *Fellow, IEEE*

Abstract—Optical imaging using independent component analysis (OPTICA) has been used for detection, 3-D localization, and cross-section imaging of a tumor inside a model human breast composed of *ex vivo* human breast tissues. OPTICA uses a multisource target illumination and multidetector signal acquisition scheme to obtain multiple spatial and angular views of the sample for target localization. Independent component analysis of the perturbations in the spatial light intensity distribution measured on the sample boundary sorts out the signal originating from individual targets. A back-projection technique estimates the cross-section of each target. The approach correctly provided the positions of a tumor located at the mid-plane and two glandular structures located at different positions within the 33-mm-thick model breast. The reconstructed cross-section images are in good agreement with known dimensions of the structures, and pathological findings.

Index Terms—Breast cancer, diffuse optical imaging, independent component analysis, near infrared (NIR) imaging, optical mammography, optical imaging using independent component analysis (OPTICA).

I. INTRODUCTION

NEAR-INFRARED (NIR) diffuse optical tomography (DOT) is an emerging technology for functional characterization of biological tissues, and has been actively investigated to image lesions in human body organs, such as human breast [1]–[3], brain [4]–[7], and joints [8], [9]. A state-of-the-art DOT illuminates the sample (consisting of targets embedded in a turbid medium) with NIR light, measures the emergent light on the boundary of the turbid medium, and uses an iterative image reconstruction method for repeatedly solving the forward model of light propagation in the medium with an updated estimation of its optical properties to match the detected light intensities.

Manuscript received September 25, 2007; revised October 28, 2007. This work was supported in part by the U.S. Army Medical Research and Materials Command, in part by the Office of Naval Research (ONR), in part by the New York State Office of Science, Technology and Academic Research (NYSTAR), and in part by the City University of New York (CUNY) organized research programs. The work of M. Xu was supported by the Research Corporation and Fairfield University. The work of M. Alrubaiee was supported by the National Science Foundation (NSF) under Advance Placement Fellowship.

M. Xu is with the Department of Physics, Fairfield University, Connecticut, CT 06824 USA (e-mail: mxu@mail.fairfield.edu).

M. Alrubaiee is with the Department of Physics, City College and the Graduate Center, City University of New York, New York, NY 10031 USA (e-mail: malrub@sci.cuny.cuny.edu).

S. K. Gayen and R. R. Alfano are with the Institute for Ultrafast Spectroscopy and Lasers, City College and the Graduate Center, City University of New York, New York, NY 10031 USA (e-mail: gayan@sci.cuny.cuny.edu; ralfano@sci.cuny.cuny.edu).

Color versions of one or more of the figures in this paper are available online at <http://ieeexplore.ieee.org>.

Digital Object Identifier 10.1109/JSTQE.2007.912831

This problem of imaging targets in a turbid medium is an ill-posed inverse problem, and *a priori* knowledge about the optical properties of the medium need to be used to obtain a unique solution at a cost of reduced resolution [10]–[13]. Various prior information such as anatomical structures obtained from X-ray or magnetic resonance imaging (MRI) and the absorption spectra of chromophores have been used to improve the imaging quality of the DOT [14]–[16]. The iterative image reconstruction is computation time intensive and reconstruction in 2-D planar sections instead of a 3-D volume is commonly practiced. Noniterative approaches have also been pursued [17]–[19]. Irrespective of these developments, reconstruction of images with adequate spatial resolution and accurate localization and characterization of the targets remain a formidable task.

We have developed an alternative approach for optical imaging using independent component analysis (OPTICA) [18], [20] that uses a multisource sample illumination and multidetector signal acquisition scheme to generate an extensive data set providing a variety of spatial and angular views of the medium. The signals from individual targets within the interrogated medium are then sorted out by using independent component analysis (ICA) based on their statistical independence. ICA is a statistical technique from information theory that is able to recover independent signals from their measured mixtures [21], [22]. ICA has been successfully applied in many biomedical applications, such as electroencephalogram (EEG) [23] and functional magnetic resonance imaging (fMRI) [24], and has been shown to be effective in separating signals from different brain activity centers. In DOT, excess light absorption or scattering by the individual targets embedded in the medium serve as the source of independent signals whose weighted mixture is recorded by a detector on the boundary of the medium. Since an independent component originating from any particular target relates directly to how light propagates from the source to the target and from the target to the detector, the recovered independent components can serve as the starting point for 3-D localization and optical characterization of individual targets in the medium. Such a staged procedure has been shown to significantly improve the sensitivity to small/weak absorptive, scattering and/or fluorescent targets, and can achieve a 3-D localization of the targets with remarkable accuracy and resolution [18], [25], [26].

The independent component is proportional to the strength of the target (the product of the difference in the absorption/scattering coefficient between the target and the background, and the volume of the target) and the convolution of the light propagators from the source to the target and from the

target to the detector. The two light propagators can be deconvoluted in the Fourier space. A 2-D cross-section image of the target is obtained by back projecting the independent component onto the transversal plane at the axial location of the target. Every independent component retrieved by ICA represents the signal from only one target with localization determined from earlier stage of analysis. So, a back projection formalism with little or no regularization can be applied to obtain a cross-section image of the target with improved spatial resolution than what is feasible in a conventional DOT.

We have previously tested the efficacy of OPTICA on samples consisting of absorbing or scattering targets within tissue phantoms and fluorescent targets in *ex vivo* tissue [18], [25], [26]. In this paper, we use OPTICA to investigate a tumor and other structures embedded in a “realistic” model breast assembled using *ex vivo* human breast tissues, as a prelude to *in vivo* breast imaging. The remainder of the paper is organized as follows. Section II presents the theoretical formalism of OPTICA and the back-projection approach for obtaining the cross-section image of a target. Section III describes the experimental arrangement, method, and parameters. Experimental results appear in Section IV. The implications are discussed in Section V.

II. THEORETICAL FORMALISM OF OPTICAL IMAGING USING INDEPENDENT COMPONENT ANALYSIS

The presence of targets (optical inhomogeneities) inside a turbid medium perturbs the spatial intensity distribution of light emergent from the medium under illumination by a probing beam. When illuminated by a point source of unit power, the change in the light intensity distribution on the boundary of the specimen due to absorptive and scattering targets can be written as [27], [28]

$$-\Delta I(\mathbf{r}_d, \mathbf{r}_s) = \int d^3\mathbf{r} \delta\mu_a(\mathbf{r}) cG(\mathbf{r}_d, \mathbf{r}) G(\mathbf{r}, \mathbf{r}_s) + \int d^3\mathbf{r} \delta D(\mathbf{r}) c\nabla_{\mathbf{r}} G(\mathbf{r}_d, \mathbf{r}) \nabla_{\mathbf{r}} G(\mathbf{r}, \mathbf{r}_s) \quad (1)$$

in the first-order Born approximation assuming that light diffuses inside the medium [29]. Here, \mathbf{r}_s and \mathbf{r}_d are the positions of the source and the detector on the boundary, $\delta\mu_a(\mathbf{r}) = \mu_a(\mathbf{r}) - \mu_{a_0}$ and $\delta D(\mathbf{r}) = D(\mathbf{r}) - D_0$ are the differences in absorption coefficient and diffusion coefficient, respectively, between the target at \mathbf{r} and the background medium, c is the speed of light in the medium, and $G(\mathbf{r}, \mathbf{r}')$ is the Green's function describing light propagation from \mathbf{r}' to \mathbf{r} inside the medium of absorption coefficient μ_{a_0} and diffusion coefficient D_0 .

OPTICA assumes each inhomogeneity within the turbid medium to be a virtual source and expresses the change of the light intensity on the boundary of the specimen as

$$-\Delta I(\mathbf{r}_d, \mathbf{r}_s) = \sum_j a_j(\mathbf{r}_d) s_j(\mathbf{r}_s) \quad (2)$$

where $s_j(\mathbf{r}_s)$ represents the j th target illuminated by the incident wave at \mathbf{r}_s and $a_j(\mathbf{r}_d)$ is the weighting matrix describing the propagation of light from the j th inhomogeneity to the detector at \mathbf{r}_d . Each absorptive inhomogeneity contributes one term in

(2), and each scattering inhomogeneity contributes three terms in (2) [18]. The detected change of the light intensity $-\Delta I$ is, hence, a linear mixture of signals where a_j and s_j can now be interpreted as the j th weighting matrix and virtual source, respectively. Owing to the statistical independence between these virtual sources, independent component analysis of $-\Delta I$ will yield a list of independent components and recover both a_j and s_j . Here, a_j and s_j are the independent intensity distribution on the detector and source planes, respectively, for the j th target. The number of the leading independent components gives the number of objects. The location of the j th target is obtained from the analysis of the retrieved independent component (s_j and a_j) that relates directly to the source-to-object and object-to-detector Green's functions $G(\mathbf{r}_j, \mathbf{r}_s)$ and $G(\mathbf{r}_d, \mathbf{r}_j)$ and the optical property of the target where \mathbf{r}_j is the position of the j th object [18], [20], [25], [26].

For the slab geometry investigated here, there are three virtual sources of specific patterns (one centrosymmetric and two dumbbell-shaped) associated with each scattering inhomogeneity, whereas only one centrosymmetric virtual source is associated with each absorptive inhomogeneity. Among the three virtual sources associated with a scattering inhomogeneity, the centrosymmetric virtual source is the strongest and more amenable to detection in a thick turbid medium [25]. The centrosymmetric virtual source and the corresponding weighting matrix are $s_j \propto G(\mathbf{r}_j, \mathbf{r}_s)$ and $a_j \propto G(\mathbf{r}_d, \mathbf{r}_j)$, and $s_j \propto \partial G/\partial z(\mathbf{r}_j, \mathbf{r}_s)$ and $a_j \propto \partial G/\partial z(\mathbf{r}_d, \mathbf{r}_j)$, respectively, for absorptive and scattering inhomogeneities. A simple least square fitting of the centrosymmetric component, such as

$$\min_{\mathbf{r}_j, \alpha_j, \beta_j} \left\{ \sum_{\mathbf{r}_s} [\alpha_j^{-1} s_j(\mathbf{r}_s) - G(\mathbf{r}_j, \mathbf{r}_s)]^2 + \sum_{\mathbf{r}_d} [\beta_j^{-1} a_j(\mathbf{r}_d) - G(\mathbf{r}_d, \mathbf{r}_j)]^2 \right\} \quad (3)$$

for the absorptive object, can be used to yield the 3-D location \mathbf{r}_j and the strength $\alpha_j \beta_j$ of the target. When *a priori* knowledge about the property of the target is not available, (3) can still be used to estimate the 3-D location of the target regardless of the absorption or scattering property of the target. This is due to the fact that $\partial G/\partial z(\mathbf{r}_j, \mathbf{r}_s) \simeq -\kappa G(\mathbf{r}_j, \mathbf{r}_s)$ and $\partial G/\partial z(\mathbf{r}_d, \mathbf{r}_j) \simeq -\kappa G(\mathbf{r}_d, \mathbf{r}_j)$, where $\kappa = \sqrt{(\mu_{a_0} - i\omega/c)/D_0}$ is chosen to have a nonnegative real part with ω the modulation frequency of the incident wave.

The signal from the j th target is simply given by $-\Delta I_j = a_j(\mathbf{r}_d) s_j(\mathbf{r}_s)$. On the other hand, the centrosymmetric signal of the j th target can be approximated as a double convolution

$$-\Delta I_j(\mathbf{r}_d, \mathbf{r}_s) = \int G(\boldsymbol{\rho}_d - \boldsymbol{\rho}, z_d, z_j) X_j(\boldsymbol{\rho}) G(\boldsymbol{\rho} - \boldsymbol{\rho}_s, z_j, z_s) d\boldsymbol{\rho} \quad (4)$$

where the integration is over the $z = z_j$ plane, X_j represents the target, and $\boldsymbol{\rho}_d$ and $\boldsymbol{\rho}_s$ are the lateral coordinates of the detector and the source, respectively. The cross-section image of the j th target X_j is a 2-D distribution of the absorption/scattering coefficient of the target on the $z = z_j$ plane. In the Fourier space,

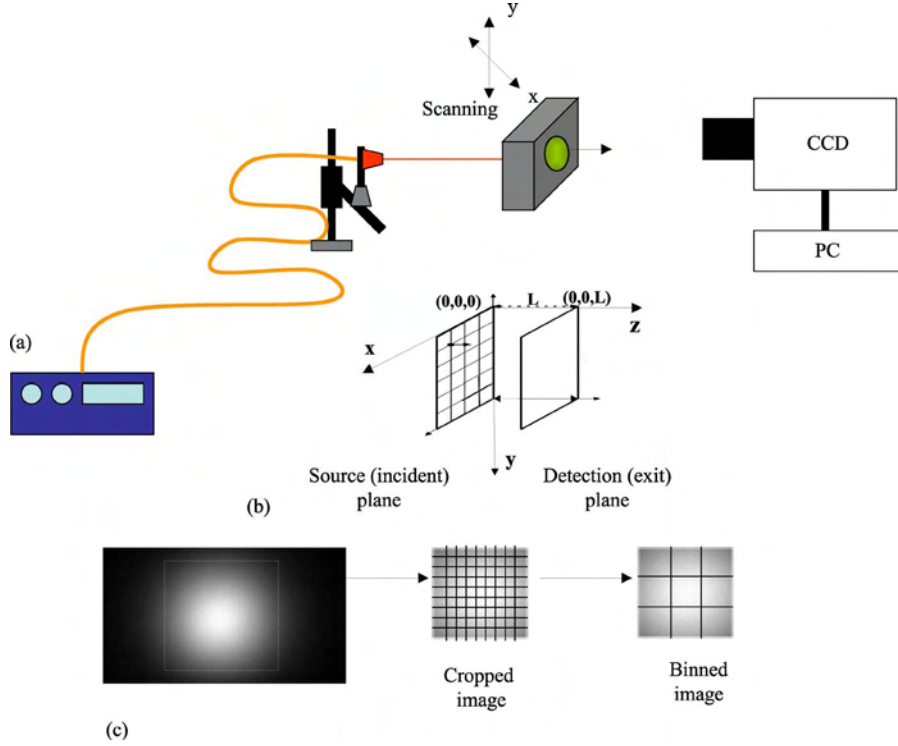


Fig. 1. (a) Schematic diagram of the experimental arrangement. CCD, charge coupled device; PC, personal computer. (b) Expanded view of the sample input (source) plane and exit (detection) plane showing the grid points in the x - y plane. (c) Typical raw CCD image of the detection plane, and how it is cropped and binned for analysis.

the target function X_j can be obtained from (4) as

$$X_j(\mathbf{q}) = -\frac{\Delta I_j(\mathbf{q} - \mathbf{q}_s, \mathbf{q}_s)}{G(\mathbf{q} - \mathbf{q}_s, z_d, z_j)G^*(\mathbf{q}_s, z_j, z_s)} \quad (5)$$

where \mathbf{q} and \mathbf{q}_s are the spatial frequency on the lateral plane and “*” denotes complex conjugate. We choose $\mathbf{q}_s = 0$ in the evaluation of the target function (5) since sources are usually much sparser than detectors in our setup where a charge-coupled device (CCD) camera is used to detect the emergent light intensity on the surface of the medium. The inverse Fourier transforms of $X_j(\mathbf{q})$ yields the high-resolution cross-section image of the j th target due to the high density of detecting pixels of the CCD. The size of the target is estimated by the full-width at half-maximum (FWHM) of the cross-section image X_j .

To sum up, OPTICA first detects and retrieves independent components corresponding to each target embedded inside a turbid medium, then obtains the 3-D location and strength of the target from these independent components, further reconstructs the cross-section image of the target on the transversal plane where the target locates, and finally, the size and the optical property of the target are estimated.

III. EXPERIMENT

The experimental arrangement for detection and localization of the tumor in the *ex vivo* model breast sample is shown in Fig. 1(a). The model breast was a 70 mm × 55 mm × 33 mm slab composed of excised female human breast tissues provided to us by National Disease Research Interchange under an Inter-

nal Review Board approval at the City College of New York. The model breast was assembled using two pieces of *ex vivo* human breast tissues. The larger piece was normal tissue that included mainly adipose tissue and streaks of fibroglandular tissues. The existence of the fibroglandular tissues was not known prior to making the measurements.

The second piece was mainly a tumor (infiltrating ductal carcinoma) with a small amount of normal tissues in the margins with an overall approximate dimension of 8 mm × 5 mm × 3 mm. An incision was made in the mid-plane (along the z -axis, which was the shorter dimension of the tissue) of the normal piece, and some amount of the normal tissue was removed from the central region making a small pouch. The tumor piece was then inserted into the pouch, and the incision was closed by moderate compression of the composite consisting of the normal tissue and the tumor along xyz -directions. The breast tissue slab was contained inside a transparent plastic box. One of the sides of the box could be moved to uniformly compress the tissue along the z -axis and hold it in position. The resulting specimen, a 70 mm × 55 mm × 33 mm slab, was treated as one entity in the subsequent imaging experiment. The position of the tumor within the slab was known since it was placed in the position as discussed earlier. One of the tests of the efficacy of this imaging approach was to see how well the known position is assessed.

A 200 μm optical fiber delivered a 784 nm, 300 mW continuous-wave beam from a diode laser for sample illumination. The beam was collimated to a 1 mm spot onto the entrance face (henceforth referred to as the “source plane”)

of the slab sample. Multiple source illumination was realized in practice by step scanning the slab sample across the laser beam in an xy array of grid points using a computer-controlled translation stage. The xy array was 22×16 with a step size of 2.0 mm. The signal from the opposite face of the sample (henceforth referred to as the “detection plane”) was collected by a camera lens and projected onto the sensing element of a cooled 16 b, 1024×1024 pixel CCD camera. Although the scanned area is $42 \text{ mm} \times 30 \text{ mm}$ on the source plane, the imaged area of the detection plane was much larger, covering the entire $70 \text{ mm} \times 55 \text{ mm}$ transverse area of the model breast. Each illuminated pixel of the CCD camera could be regarded as a detector. For illumination of every scanned point on the source plane, the CCD camera recorded the diffusely transmitted 2-D intensity pattern on the detection plane. Each image acquisition took 100 ms, and one stepping of the translational stage took 1 s. A total of 352 images were completed within 7 min. The OPTICA reconstruction and cross-section imaging is expected to be completed within 2 min once fully automated.

IV. RESULTS

A typical 2-D raw image of transmitted light intensity distribution on the detector plane for illumination at a typical scanning position is shown in Fig. 1(c). The average of all the 22×16 images was used to obtain the optical property of the slab of breast tissue. The radial profile of the intensity of the transmitted light on the average image was fitted to that predicted by a diffusion model of light propagation inside a slab. The transport mean free path was assumed to be 1 mm, the value for a typical human breast tissue at 785 nm. The reduced scattering coefficient was then 1 mm^{-1} . From the decay of the radial profile of the intensity of the transmitted light, the average absorption coefficient of the entire model breast is found to be $\mu_a = 0.0039 \text{ mm}^{-1}$. Each raw image is first cropped to retain the region within the window of $50.4 \text{ mm} \times 51.3 \text{ mm}$ (out of a total $70 \text{ mm} \times 55 \text{ mm}$ transverse area of the model breast) over which image reconstruction would be performed. The size of 1 pixel in the raw image is $187 \mu\text{m} \times 187 \mu\text{m}$. The raw images are binned by merging 5×5 pixels into one to enhance the SNR, resulting in a total of 352 images of 54×55 pixels each. All the binned images corresponding to illumination of the grid points in sequence were then stacked, and used as input for independent component analysis.

The independent light intensity distributions obtained by OPTICA is displayed in Fig. 2(a). The 3-D location of the targets were obtained from least squares fitting using (3). The fittings of the independent light intensities over lines passing through the maximum value and along the horizontal direction are displayed in Fig. 2(b). The tumor C is found at 14.8 mm from the detection plane and centered at (33.3, 21.5, 18.2) mm. In addition, two glandular sites were identified. The first glandular site A is found to be located at 2.5 mm from the detection plane and centered at (11.2, 22.4, 30.5) mm; the second glandular site B is at 14.6 mm from the detection plane and centered at (21.5, 37.3, 18.4) mm. Comparison of known and 3-D positions ob-

tained from OPTICA for the cancer site and two glandular sites is given in Table I.

The cross-section image of the tumor obtained from a 2-D inverse Fourier transform of (5) is shown in Fig. 3 (left pane). The right pane of Fig. 3 displays the intensity profiles of the cross-section image along the x - and y -directions denoted by the white dashed lines. The FWHM values of the intensity profiles yield estimates of the lateral dimensions of the tumor to be $10.3 \text{ mm} \times 7.4 \text{ mm}$, while the known dimensions are $8 \text{ mm} \times 5 \text{ mm}$. Histological micrograph of the suspect site confirmed tumor. Similar back-projection cross-sectional images and histological micrographs were obtained (not shown here) for the glandular tissues as well and their transverse sizes were estimated from OPTICA. The existence, location, and size of the glandular tissues were not known *a priori*. The glandular structure A near surface is estimated to be 2.7 and 1.6 mm in size along the x - and y -directions from the cross-section image, respectively. The size of the glandular structure B at the midplane is 8.7 and 9.2 mm in size along the x - and y -directions, respectively.

Low regularization was used in generating the cross-section images in Fig. 3 to achieve maximal spatial resolution. The artifacts in the cross-section images can be suppressed with a higher regularization at a cost of lower spatial resolution. Since the target has been localized in the earlier stage of analysis, the target will not be confused with artifacts in the cross-section images and low regularization is beneficial here.

The investigated *ex vivo* breast sample contained minimal amount of blood, and hence, the reconstructed images are for the scattering property of the sample. The change of the reduced scattering coefficient μ'_s for the targets can further be estimated from the reconstructed independent components for the sites A, B and C. The value of $\delta\mu'_s$ is given by the ratio of the strength of the target and its volume. The sites A and B have lower scattering while the site C has enhanced scattering compared to the background (mainly adipose tissue). The values of $\delta\mu'_s$ are ~ 0.2 and $\sim -0.4 \text{ mm}^{-1}$ for the tumor and glandular tissues, respectively. Subsequent pathological analysis confirmed the site C as infiltrating ductal carcinoma, and identified the other two structures as glandular breast tissues.

V. DISCUSSION

The results of the experiments clearly demonstrate that OPTICA can locate the tumor inside the model breast with high accuracy. As can be seen from Table I, the lateral positions of the tumor agree within 0.5 mm, while the axial position agree within ~ 1 mm of the known values. Similar high accuracy in the respective positions of the two pieces of glandular tissues is observed as well. The accuracy of the lateral positions does not depend significantly on the depth of the targets, while that of the axial position shows a weak dependence. For the target located close to the detection plane (glandular site A at a distance of 2.5 mm from the detection plane), the axial position is determined exactly, while for targets in the midplane that are much more challenging to locate, the accuracy is within 1 mm. Given

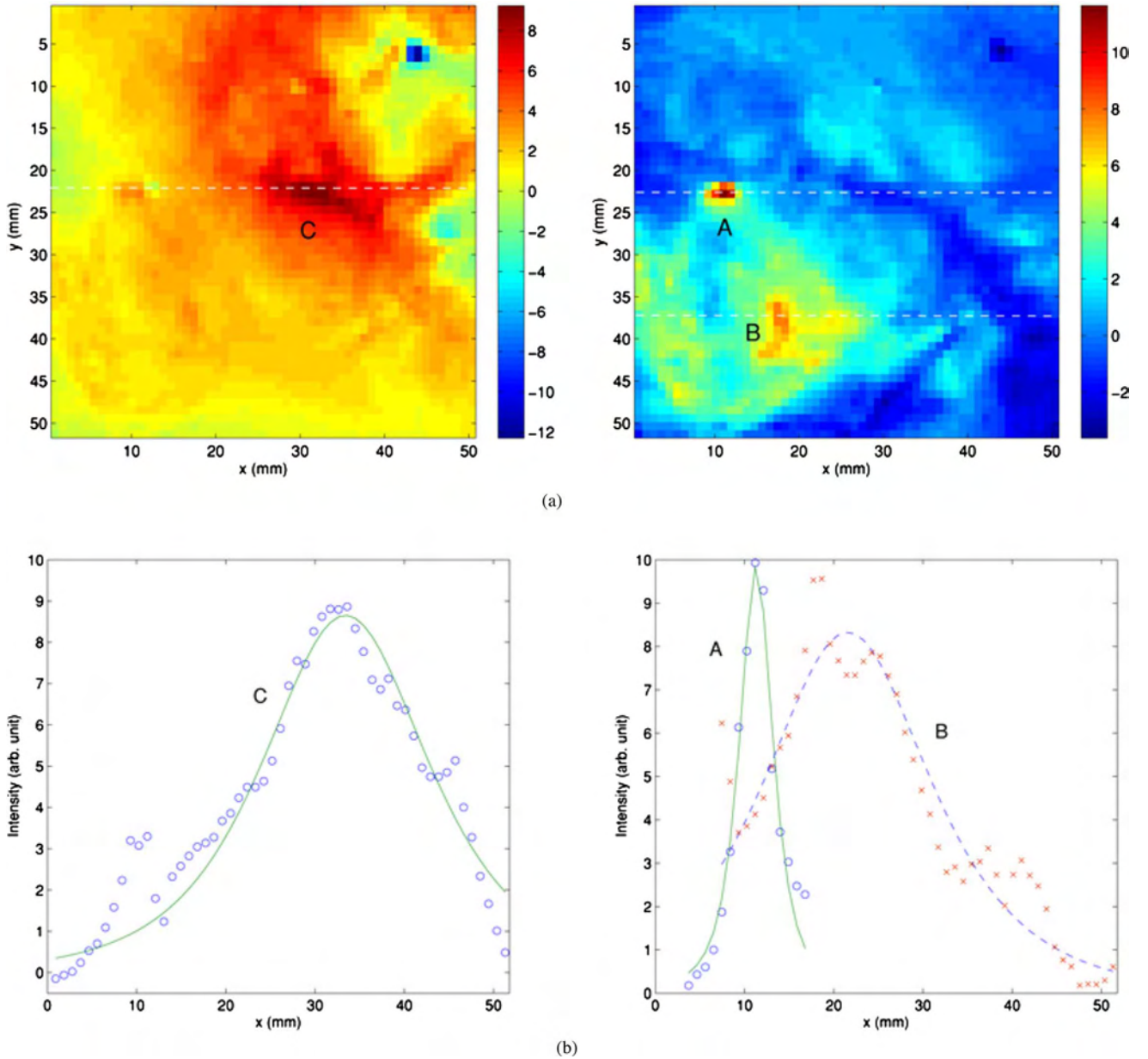


Fig. 2. (a) Independent intensity distribution on the detector plane ($z = 33$ mm) obtained by OPTICA for the tumor C (left pane) and the glandular structures A and B (right pane). (b) Corresponding bottom panes show the Green's function fits (solid lines) to the horizontal spatial profile (denoted by circles and crosses) through the center of the intensity distributions along the dashed lines.

TABLE I
COMPARISON OF KNOWN AND OPTICA ESTIMATED TARGET LOCATIONS

Target	Known Position (x, y, z) (mm)	OPTICA Estimated Position (x, y, z) (mm)
Cancer Site (C)	(33,21,16.9)	(33.3,21.5,18.2)
Glandular Site (A)	(11,22,30.5)	(11.2,22.4,30.5)
Glandular Site (B)	(21,37,17)	(21.5,37.3,18.4)

that light propagation is highly diffusive in breast tissues, this level of accuracy is quite significant.

The back-projection formalism estimates the FWHM values of the lateral dimension of the tumor to be 10.3 and 7.4 mm in size along the x - and y -directions, respectively, whereas the known dimension is 8 mm \times 5 mm. This result is expected due

to diffusion of light in the tissue, and is in line with the results that we obtained in our earlier OPTICA studies [26].

Another important finding was that OPTICA predicted different scattering properties for the adipose tissue (medium), the tumor, and the glandular tissues. The glandular tissues were found to be less scattering than the adipose tissues at the wavelength of interrogation, i.e., 784 nm. The tumor was found to be more scattering. These observations are consistent with the known literature values of scattering properties of different types of tissues [30].

The nature of the inhomogeneity (either absorptive or scattering or mixed) can be discerned by OPTICA with continuous-wave measurement when the SNR is high [20], [25]. When the SNR is not favorable, the recovered independent component

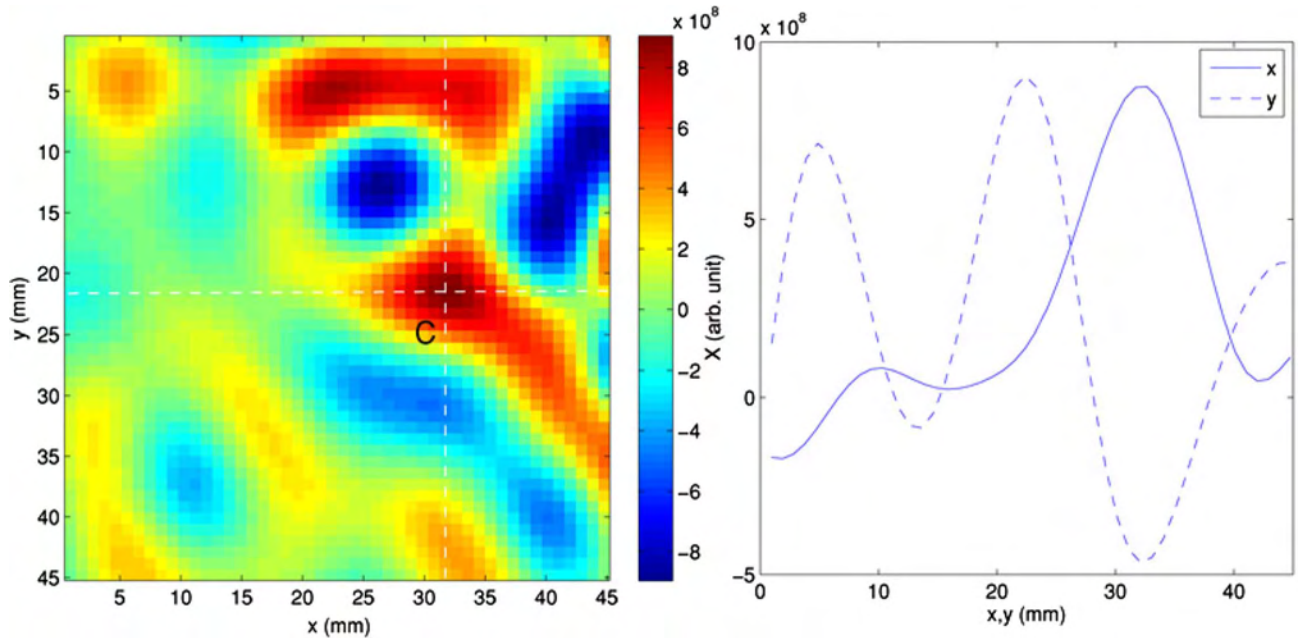


Fig. 3. Cross-section image of the tumor at the $z = 18.2$ mm plane formed by back-projection (left pane). Right pane: Spatial profiles of the cross-section image along the x - and y -directions shown by the white dashed lines (right pane). The FWHM of the cancer site is 10.3 and 7.4 mm along the x - and y -directions, respectively.

will be due to both absorption and scattering perturbations at the site of the inhomogeneity. The strength of the target will be proportional to $\delta\mu_a + \kappa^2\delta D = \delta\mu_a + (\mu_{a_0} - i\omega/c)\delta D/D_0$, which provides a way to discriminate between absorption and scattering if measurements of multiple modulation frequencies ω are available. The capability of OPTICA for separating absorption from scattering inhomogeneities can be significantly improved with a time-domain or frequency-domain measurement. Another enabling factor will be carrying out multispectral OPTICA studies for potential diagnostic information.

OPTICA can be used for fluorescent targets as well [26]. The same experimental arrangement may be used, except for the introduction of filters to block the excitation beam and to transmit the fluorescence light. What is even more interesting is that, a beam-splitter and two detectors combination with appropriate filters may be used to simultaneously pursue absorption/scattering OPTICA and fluorescence OPTICA studies of biological samples for obtaining coregistered information from dual probes.

OPTICA is suited to detect small objects. Given its ability to identify low-contrast small objects, the approach is expected to be especially useful for the detection of breast and prostate tumors at their early stages of growth.

ACKNOWLEDGMENT

The authors acknowledge Dr. W. Cai for his helpful discussions.

REFERENCES

- [1] B. Chance, S. Nioka, J. Zhang, E. F. Conant, E. Hwang, S. Briest, S. G. Orel, M. D. Schnall, and B. J. Czerniecki, "Breast cancer detection based on incremental biochemical and physiological properties of breast cancers: A six-year, two-site study," *Acad. Radiol.*, vol. 12, pp. 925–933, Aug. 2005.
- [2] R. Choe, A. Corlu, K. Lee, T. Durduran, S. D. Konecky, M. Grosicka-Koptyra, S. R. Arridge, B. J. Czerniecki, D. L. Fraker, A. DeMichele, B. Chance, M. A. Rosen, and A. G. Yodh, "Diffuse optical tomography of breast cancer during neoadjuvant chemotherapy: A case study with comparison to MRI," *Med. Phys.*, vol. 32, pp. 1128–1139, Apr. 2005.
- [3] B. Brooksby, B. W. Pogue, S. Jiang, H. Dehghani, S. Srinivasan, C. Kogel, T. D. Tosteson, J. Weaver, S. P. Poplack, and K. D. Paulsen, "Imaging breast adipose and fibroglandular tissue molecular signatures by using hybrid MRI-guided near-infrared spectral tomography," *Proc. Natl. Acad. Sci. USA*, vol. 103, pp. 8828–8833, Jun. 2006.
- [4] J. C. Hebden, A. Gibson, T. Austin, R. M. Yusof, N. Everdell, D. T. Delpy, S. R. Arridge, J. H. Meek, and J. S. Wyatt, "Imaging changes in blood volume and oxygenation in the newborn infant brain using three-dimensional optical tomography," *Phys. Med. Biol.*, vol. 49, pp. 1117–1130, Apr. 2004.
- [5] T. Durduran, G. Yu, M. G. Burnett, J. A. Detre, J. H. Greenberg, J. Wang, C. Zhou, and A. G. Yodh, "Diffuse optical measurement of blood flow, blood oxygenation, and metabolism in a human brain during sensorimotor cortex activation," *Opt. Lett.*, vol. 29, pp. 1766–1768, Aug. 2004.
- [6] M. A. Franceschini, D. K. Joseph, T. J. Huppert, S. G. Diamond, and D. A. Boas, "Diffuse optical imaging of the whole head," *J. Biomed. Opt.*, vol. 11, no. 5, pp. 054007-1–054007-10, 2006.
- [7] A. P. Gibson, T. Austin, N. L. Everdell, M. Schweiger, S. R. Arridge, J. H. Meek, J. S. Wyatt, D. T. Delpy, and J. C. Hebden, "Three-dimensional optical tomography of passive motor evoked responses in the neonate," *Neuroimage*, vol. 30, pp. 521–528, Apr. 2006.
- [8] Y. Xu, N. Iftimia, H. Jiang, L. L. Key, and M. B. Bolster, "Three-dimensional diffuse optical tomography of bones and joints," *J. Biomed. Opt.*, vol. 7, pp. 88–92, 2002.
- [9] A. H. Hielscher, "Optical tomographic imaging of small animals," *Curr. Opin. Biotechnol.*, vol. 16, pp. 79–88, Feb. 2005.
- [10] A. N. Tikhonov and A. V. Groncharsky Eds., *Ill-Posed Problems in the Natural Sciences*. Moscow, Russia: MIR, 1987.
- [11] S. R. Arridge, "Optical tomography in medical imaging," *Inverse Prob.*, vol. 15, pp. R41–R93, 1999.
- [12] X. Intes and B. Chance, "Non-pet functional imaging techniques: Optical," *Radiol. Clin. North Amer.*, vol. 43, no. 1, pp. 221–234, Jan. 2005.
- [13] A. P. Gibson, J. C. Hebden, and S. R. Arridge, "Recent advances in diffuse optical imaging," *Phys. Med. Biol.*, vol. 50, pp. R1–R43, Feb. 2005.

- [14] V. Ntziachristos, A. G. Yodh, M. D. Schnall, and B. Chance, "MRI-guided diffuse optical spectroscopy of malignant and benign breast lesions," *Neoplasia*, vol. 4, no. 4, pp. 347–354, 2002.
- [15] A. Corlu, T. Durduran, R. Choe, M. Schweiger, E. M. C. Hillman, S. R. Arridge, and A. G. Yodh, "Uniqueness and wavelength optimization in continuous-wave multispectral diffuse optical tomography," *Opt. Lett.*, vol. 28, pp. 2339–2341, Dec. 2003.
- [16] S. Srinivasan, B. W. Pogue, B. Brooksby, S. Jiang, H. Dehghani, C. Kogel, W. A. Wells, S. P. Poplack, and K. D. Paulsen, "Near-infrared characterization of breast tumors in vivo using spectrally-constrained reconstruction," *Technol. Cancer Res. Treat.*, vol. 4, pp. 513–526, Oct. 2005.
- [17] W. Cai, S. K. Gayen, M. Xu, M. Zavallos, M. Alrubaiee, M. Lax, and R. R. Alfano, "Optical tomographic image reconstruction from ultrafast time-sliced transmission measurements," *Appl. Opt.*, vol. 38, no. 19, pp. 4237–4246, 1999.
- [18] M. Xu, M. Alrubaiee, S. K. Gayen, and R. R. Alfano, "Three-dimensional localization and optical imaging of objects in turbid media using independent component analysis," *Appl. Opt.*, vol. 44, pp. 1889–1897, 2005.
- [19] Z.-M. Wang, G. Y. Panasyuk, V. A. Markel, and J. C. Schotland, "Experimental demonstration of an analytic method for image reconstruction in optical diffusion tomography with large data sets," *Opt. Lett.*, vol. 30, pp. 3338–3340, Dec. 2005.
- [20] M. Xu, M. Alrubaiee, S. K. Gayen, and R. R. Alfano, "Optical imaging of turbid media using independent component analysis: Theory and simulation," *J. Biomed. Opt.*, vol. 10, pp. 051705-1–051705-12, 2005.
- [21] P. Comon, "Independent component analysis—A new concept?," *Signal Process.*, vol. 36, pp. 287–314, 1994.
- [22] A. J. Bell, "Information theory, independent component analysis, and applications," in *Unsupervised Adaptive Filtering*, vol. I, S. Haykin, Ed. New York: Wiley, 2000, pp. 237–264.
- [23] R. Vigário, J. Särelä, V. Jousmäki, M. Hämäläinen, and E. Oja, "Independent component approach to the analysis of EEG and MEG recordings," *IEEE Trans. Biomed. Eng.*, vol. 47, no. 5, pp. 589–593, May 2000.
- [24] B. B. Biswal and J. L. Ulmer, "Blind source separation of multiple signal sources of f MRI data sets using independent component analysis," *J. Comput. Assist. Tomogr.*, vol. 23, no. 2, pp. 265–271, 1999.
- [25] M. Alrubaiee, M. Xu, S. K. Gayen, and R. R. Alfano, "Tomographic imaging of scattering objects in tissue-like turbid media using independent component analysis," *Appl. Phys. Lett.*, vol. 87, pp. 191112-1–191112-3, 2005.
- [26] M. Alrubaiee, M. Xu, S. K. Gayen, and R. R. Alfano, "Localization and cross-section reconstruction of fluorescent targets in *ex vivo* breast tissue using independent component analysis," *Appl. Phys. Lett.*, vol. 89, pp. 133902-1–133902-3, 2006.
- [27] M. A. O'Leary, D. A. Boas, B. Chance, and A. G. Yodh, "Experimental images of heterogeneous turbid media by frequency-domain diffusing-photon tomography," *Opt. Lett.*, vol. 20, pp. 426–428, 1995.
- [28] M. Xu, M. Lax, and R. R. Alfano, "Time-resolved Fourier optical diffuse tomography," *J. Opt. Soc. Amer. A*, vol. 18, no. 7, pp. 1535–1542, 2001.
- [29] P. M. Morse and H. Feshbach, *Methods of Theoretical Physics*, vol. I/II. New York: McGraw-Hill, 1953.
- [30] M. Alrubaiee, S. K. Gayen, R. Alfano, and J. A. Koutcher, "Spectral and temporal near-infrared imaging of *ex vivo* cancerous and normal human breast tissues," *Tech. Cancer Res. Treat.*, vol. 4, pp. 457–469, 2005.



Min Xu received the B.S. and M.S. degrees from Fudan University, Shanghai, China, in 1992 and 1995, respectively, and the Ph.D. degree from the City University of New York, New York, in 2001, all in physics.

He is currently an Assistant Professor in the Department of Physics, Fairfield University, Connecticut. His recent work in biomedical optics has been on modeling light scattering by cells and human tissues, and developing optical spectroscopic and tomographic methods for cancer detection. He is the

author or coauthor of more than 35 peer-reviewed papers published in various international journals and also the coauthor of the book *Random Processes in Physics and Finance* (Oxford University Press, 2006). His current research interests include wave scattering and propagation in random media and coherent phenomenon, radiative transfer of polarized light, random processes and Monte Carlo methods, biomedical optics, and inverse problems in applied physics and engineering.



Mohammad Alrubaiee received the B.Sc. degree in electric engineering and the M.Sc. degree in physics from the City College, City University of New York, in 1993 and 1999, respectively, and the Ph.D. degree in physics from the Graduate Center of the City University of New York, in 2007.

He is currently a Research Associate at the Institute for Ultrafast Spectroscopy and Laser, City College, City University of New York. His current research interests include time-resolved and optical spectroscopic imaging of biomedical media and optical tomography. He is the author or coauthor of more than 12 articles published in various refereed journals.



S. K. Gayen received the B.Sc. (Hons.) and M.Sc. degrees from the University of Dacca, Dacca, Bangladesh, in 1975 and 1977, respectively, and the Ph.D. from the University of Connecticut, Storrs, in 1984.

He is currently a Professor of physics at the City College and the Graduate Center of the City University of New York, New York. His current research interests include optical biomedical imaging, imaging of targets in turbid media, tunable solid-state lasers, spectroscopy of impurity ions in solids, nonlinear optics, ultrafast laser spectroscopy, and optical spectroscopy and microscopy of nanocomposites.

Dr. Gayen is a member of the American Physical Society and the Optical Society of America.



R. R. Alfano (M'87–SM'89–F'01) received the B.S. and M.S. degrees from Fairleigh Dickinson University, Hackensack, NJ, in 1963 and 1964, respectively, and the Ph.D. degree from New York University, in 1972, all in physics.

He is currently a Distinguished Professor of science and engineering at the City College and the Graduate Center of the City University of New York, New York. He is also the Director of the Institute for Ultrafast Spectroscopy and Lasers and the DoD Center for Nanoscale Photonic Emitters and Sensors

at the City College. His current research interests include optical biomedical imaging, photon propagation through turbid media, ultrafast laser science and technology, ultrafast supercontinuum generation, tunable solid-state lasers, nonlinear optics, laser-induced shock waves, terahertz spectroscopy, as well as dynamical processes in semiconductors, dielectric crystals, molecular systems, polymers, and biological systems. He is the author or coauthor of more than 650 papers published in various international journals, edited four books and several conference proceedings, and organized several major conferences. He is the holder of 101 patents.

Dr. Alfano is a Fellow of the American Physical Society, IEEE and the Optical Society of America.

Detection of a target in a highly scattering turbid medium using near-infrared center of intensity time gated imaging

Yimin Wang, S. K. Gayen, M. Alrubaiee, and R. R. Alfano

Institute for Ultrafast Spectroscopy and Lasers, Department of Physics,

The City College of New York, New York, 10031

Abstract

A near-infrared optical imaging approach for locating a target embedded in a turbid medium is introduced. The target localization is based on an analysis of the spatial variation of the transmitted light intensity distribution for illumination at different positions on the sample boundary. The approach is used to detect and generate a two-dimensional image of an absorbing target embedded inside a model scattering medium of thickness 50 times the transport mean free path of the medium, as well as, a piece of porcine liver embedded in porcine tissue.

Key words:

Optical imaging, time-resolved imaging, turbid medium, near-infrared imaging

Optical detection of a target embedded in a highly-scattering turbid medium is a challenging problem with diverse potential applications, such as, imaging of a tumor in human breast, mines in shallow coastal water, and airborne surveillance through cloud or fog cover. Light multiple scattered by the intervening medium encroaches into the region of geometrical shadow, and obscures the direct transillumination image of the target. A variety of time-resolved, frequency-domain, and continuous wave methods for direct imaging and inverse reconstruction of images has evolved over the years.¹⁻⁸ Most of these approaches are difficult to implement because those require complex experimental arrangements, sophisticated analytical schemes and time-intensive numerical algorithms for generation of images.

In this article, we introduce a transillumination imaging approach for prompt target detection. The approach is based on the premise that a target (that is, an optical inhomogeneity) within the turbid medium alters the propagation of light through the medium. Consequently, the spatial distribution of the output light intensity (SDOLI) is different with an embedded target than that without it.

The SDOLI depends on where and how the turbid medium is illuminated, as illustrated schematically in Fig. 1. In the slab geometry of Fig.1, a narrow beam of light is incident on the source plane ($z = 0$ plane). A fraction of the beam propagates diffusely in the z -direction, and emerges through the opposite side, i.e., the detection plane ($z = d$ plane). The SDOLI at the detection plane is a two-dimensional ($2-D$) intensity distribution that can be measured by a charge coupled device (CCD) camera. The black ellipse represents a target in the medium, and the gray spot at the detection plane is the shadow of the target. For a uniform scattering medium without the target, the intensity distribution of the diffused light inside the medium is symmetric about the incident direction, as shown by the solid curve of intensity distribution in Fig. 1. When

there is a target with optical properties different than that of the turbid medium, as shown by the black ellipse, the transmitted light intensity distribution will be altered because of scattering and/or absorption by the target. Consequently, the spatial distribution of the light intensity at the detection plane will be distorted and different with an embedded target than that without it, as shown schematically by the dashed curve. It is possible to locate the target within the turbid medium through an analysis of this intensity variation. The analysis starts with a calculation of the center of the SDOLI at the detection plane given by

$$M = \frac{\int_{x_1}^{x_2} Ix dx}{\int_{x_1}^{x_2} I dx}, \quad (1)$$

where I is the light intensity recorded by a CCD camera and x is the position. For a uniform medium illuminated by a point source, the transmitted intensity distribution centers on the incident direction. When the target is located to the right side of the incident beam line, as shown in Fig. 1, it will introduce a shadow at the right part of the output beam and lead to a decrease and distortion in the output intensity distribution. This results in the movement of the intensity peak of the output beam to the left direction. Consequently, the center of intensity distribution M will show a left (negative) movement. When the target is to the left of the incident beam, it will introduce a shadow at the left side of the output beam and M will show a right (positive) movement. When the object is on the incident beam path, the center of intensity of the output beam profile would be same as that without target inside, but the peak intensity would be reduced.

The experimental arrangement for realizing the approach in practice is shown in Fig. 2. The scattering medium was a suspension of Intralipid-10% in water, with an estimated reduced

scattering coefficient, $\mu_s' \sim 1.168 \text{ mm}^{-1}$ (transport length 0.86 mm) and an absorption coefficient of 0.0021 mm^{-1} at 800 nm.⁹ The Intralipid-10% suspension was held in a 240 mm x 160 mm x 65 mm rectangular glass container. A 10 mm x 10 mm x 3 mm neutral density filter (absorption coefficient 0.23 mm^{-1} at 800 nm) was placed inside the medium as the target.

The scattering medium was illuminated by 800 nm, 200 ps, 1 kHz repetition rate pulses from a Ti:sapphire laser and regenerative amplifier system. The amplified pulses were not compressed. The average beam power was 150 mW and the beam spot size was approximately 2 mm. The laser beam was incident along the z -axis into one of the 240 mm x 160 mm flat faces of the container. The 2- D intensity distribution of light emergent from the opposite end face of the cell was recorded by an ultrafast gated intensified camera system (UGICS). The UGICS provides an electronic time gate whose full width at half maximum (FWHM) duration can be set as short as 80 ps. The gate position could be varied over a 20 ns range with a minimum step size of 25 ps. The sample cell was mounted on a translation stage for lateral scanning. The input beam and the UGICS were not scanned. An 80 mm linear region of the sample was scanned in 4 mm steps providing 21 data points.

Fig. 3 (a) shows the temporal profile of the transmitted pulse without the target inside the medium. The 80 ps time gate was centered at a time that corresponded to the peak position of the transmitted pulse profile indicated by an arrow on the profile. Two-dimensional images were recorded at each scanning position, a typical image being shown in Fig. 3(b). Fig. 3(c) shows the horizontal intensity profiles obtained by integrating a 3-pixel wide area around the white dashed line shown in Fig. 3(b). The solid line in Fig. 3(c) is a spatial profile without the target inside the medium, while the dotted line is the corresponding profile when the target was on the incident

beam path. The solid (dashed) line in Fig. 3(d) presents the spatial profile when the target was to the right (left) of the incident beam path.

For a quantitative evaluation of this intensity distortion, the spatial intensity profiles were obtained for all 21 scanning positions, and the corresponding centers of the intensity distributions, M_i were calculated using Eq. (1). The average of the 21 profiles was then obtained, and its center of intensity was calculated and taken to be the reference, M_0 . The differences, $\Delta M_i = M_i - M_0$, were obtained and plotted as a function of scanning position as shown by the squares in Fig. 4. ΔM is negative in the left side of this center-of-intensity curve (CIC), passes through a minimum, reaches zero, rises to a positive maximum and tends towards zero further out to the right. The curve has inversion symmetry about the zero position. The zero point shows the position of the embedded target. When the scanning beam is far away from the object, ΔM is close to zero. The dashed curve in Fig. 4 shows the first derivative of the center of intensity $Q = d(\Delta M)/dx$, which peaks at the target position.

These results show that as the distance between the input beam and target increases, ΔM changes quickly at first. The maximum value of Q occurs at the position when the scanning beam passes through the target. After reaching the optimal value, ΔM changes slowly towards zero. When the target is far away from the input beam, its influence is small, and the intensity distribution does not change. The FWHM of Q vs. scan position curve in Fig. 4 is approximately 12.6 mm, which is close to the real width of the target, 10mm.

The potential of this approach for optical biomedical imaging was next explored. The target was a 5 mm x 5 mm x 5 mm piece of porcine liver placed inside a 150 mm x 90 mm x 50 mm slab of porcine tissue held in a rectangular plastic cell. The center of the target was at a distance of 25 mm from both the entrance and the exit faces of the porcine tissue. A 100 mm x

60 mm inner region of the sample was scanned across the incident laser beam. The sample cell was scanned with a step size of 4 mm along the x direction (100 mm segment). The cell was then stepped by 3 mm along the y direction, and the x -scan was repeated. The scanning pattern continued until the entire region was scanned. Time-gated 2-D images were recorded for each scanning position. CIC curves were generated for every scan along the x direction, and the value of Q was estimated for each scanning position. Plotting of Q vs. scan position (x, y) generated a 2-D gray-scale pseudo-color image as shown in Fig. 5(a). The dark area with high Q value represents the porcine liver specimen that absorbed 800-nm light more strongly than the porcine muscle tissue. Fig. 5(b) shows a spatial profile of the image was obtained by integrating a 3-pixel wide area around the white dashed line in Fig. 5(a) The FWHM of the profile is 10 mm, which is larger than the target width of 5 mm, but comparable to the resolution that other optical imaging methods obtain.⁵

In summary, a method based on analysis of the transmitted light intensity distribution has been introduced for obtaining lateral position and 2-D images of an absorbing target in a highly scattering turbid medium including biological tissues.

The authors acknowledge Wei Cai for helpful discussions. The research is supported in part by grant W81XWH-04-1-0461 from U. S. Army Medical Research and Material Command.

References

1. J. C. Hebden, S. R. Arridge, and D. T. Delpy, "Optical imaging in medicine: I experimental techniques," *Phys. Med. Biol.* **42**, 825-840, (1997).
2. R. R. Alfano, X. Liang, L. Wang, and P. P. Ho, "Time resolved imaging of translucent droplets in highly scattering turbid media," *Science* **264**, 1913-1915 (1994).
3. L. Wang, P.P. Ho, C. Liu, G. Zhang, R. R. Alfano, "Ballistic 2-D imaging through scattering walls using an ultrafast optical kerr gate," *Science* **253**, 769-771, (1991).
4. O'Leary M. A., Boas, D.A., Chance, B., and Yodh, A. G. Experimental images of heterogeneous turbid media by frequency-domain diffusing-photon tomography. *Opt. Lett.* **20**, 426-428 (1995).
5. Arridge, S. R.. Optical tomography in medical imaging. *Inverse Probl.* **15**, R41–R93 (1999).
6. W. Cai, S. K. Gayen, M. Xu, M. Zevallos, M. Al., M. Lax, and R. R. Alfano, "Optical tomography image reconstruction from ultrafast time sliced transmission measurements," *Appl. Opt.* **38**, 4237-4246, (1999).
7. D. Grosenick, H. Wabnitz, H. H. Rinneberg, K. T. Moesta, and P.M. Schlag," Development of a time-domain optical mammography and first *in vivo* applications," *Appl. Opt.* **38**, 2927-2943, (1999).
8. H. Dehghani, B. W. Pogue, S. P. Poplack, and K. D. Paulsen, "Multiwavelength three-dimensional near-infrared tomography of the breast: initial simulation, phantom, and clinical results," *Appl. Opt.*, **42**, 135-145, (2003)
9. H. J. van Staveren, C. J. M. Moes, J. van Merle, S. A. Prahl, and M. J. C. van Gemert, "Light scattering in Intralipid-10% in the wavelength range of 400-1100 nm," *Appl. Opt.* **30**, 4507-4514 (1991).

Figure Captions

Fig. 1. A schematic diagram of the diffuse light transmission through a turbid medium showing the target and the “shadow.” The inset at the top shows intensity spatial intensity distribution without the target (solid curve) and with the target (dashed curve).

Fig. 2. A schematic diagram of the experimental arrangement (Key: PS = pulse stretcher, RGA= regenerative amplifier, UGICS = ultrafast gated intensified camera system)

Fig. 3. (a) Temporal profile of the transmitted pulse. The arrow indicates the gate position. (b) A typical time-gated image (2-D intensity distribution) of the output plane. (c) Spatial intensity profile without the target (solid line), and with the target (dotted line). (d) Similar spatial profiles as in (c), except the solid (dotted) curve corresponds to the target being located to the right (left) of the incident beam line. The arrows C , C_L , and C_R represent the peak intensity positions in the corresponding spatial profiles.

Fig. 4. Variation of the center of intensity distribution (ΔM) and its first derivative Q as a function of the scan position

Fig. 5. (a) Two-dimensional image of a 5 mm x 5 mm x 5 mm piece of porcine liver embedded inside a slab of porcine tissue; (b) horizontal spatial profile of the image.

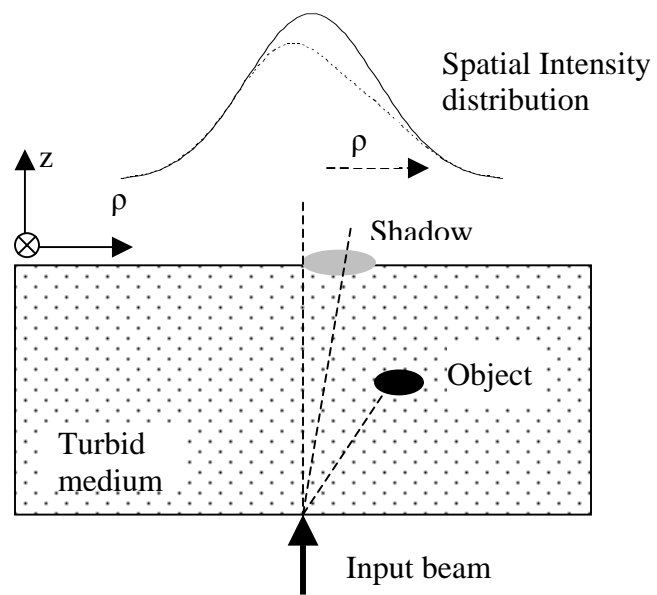


Fig. 1

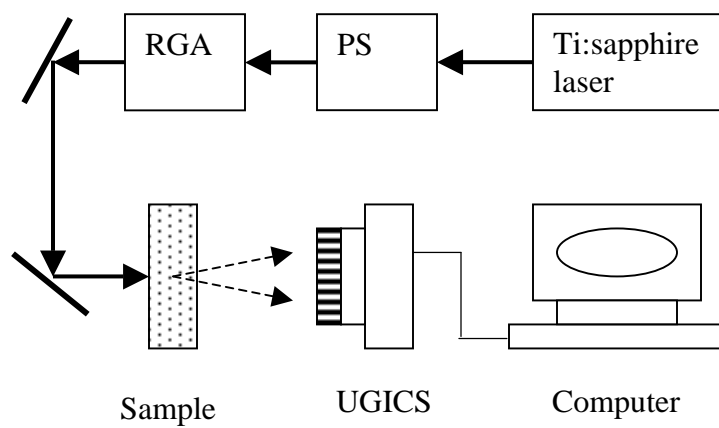


Fig. 2

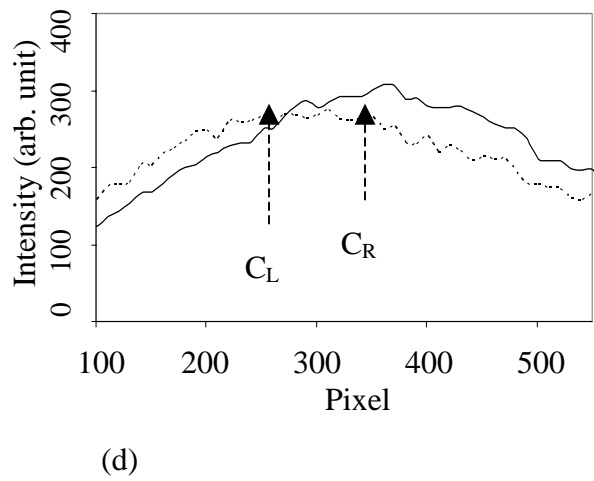
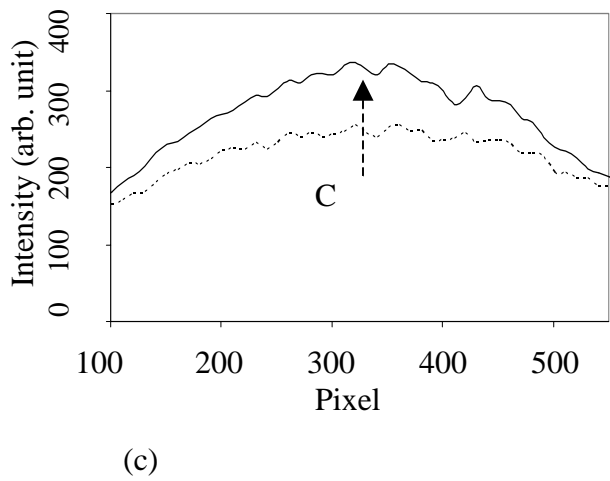
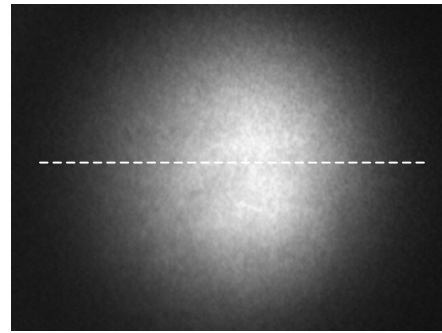
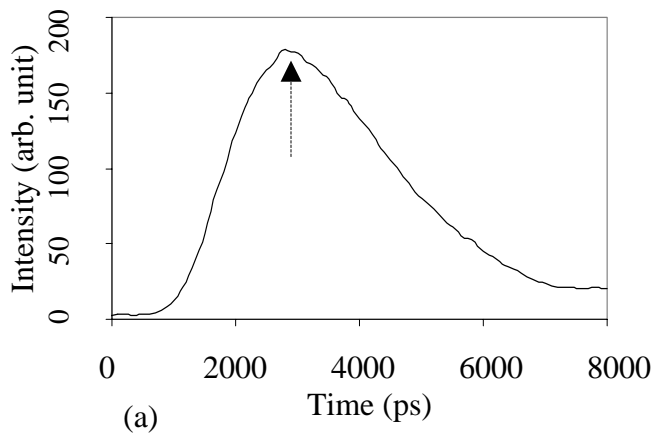


Fig. 3

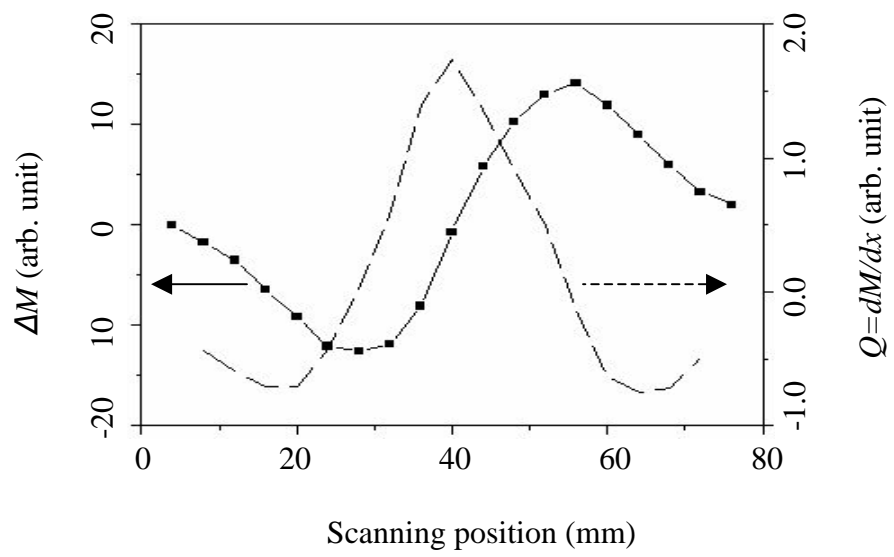


Fig. 4

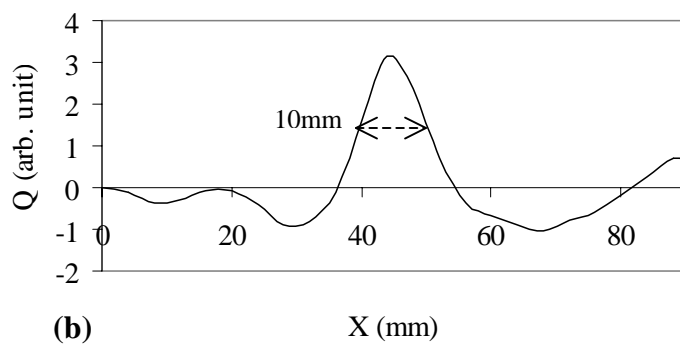
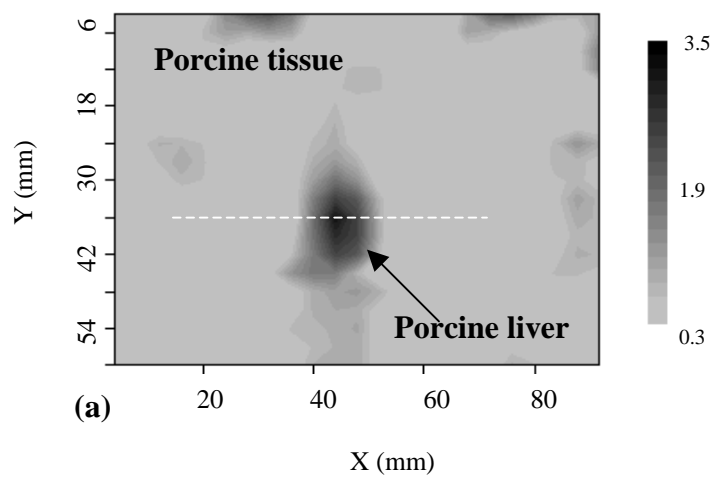


Fig. 5